Title

Surface Oxidation of Graphene Oxide Determines Membrane Damage, Lipid Peroxidation, and Cytotoxicity in Macrophages in a Pulmonary Toxicity Model

Journal

ACS Nano, 12(2)

ISSN

1936-0851

Authors

Li, Ruibin
Guiney, Linda M
Chang, Chong Hyun
et al.

Publication Date

2018-02-27

DOI

10.1021/acsnano.7b07737

Peer reviewed

HHS Public Access

Author manuscript

ACS Nano. Author manuscript; available in PMC 2019 February 27.

Published in final edited form as:

ACS Nano. 2018 February 27; 12(2): 1390–1402. doi:10.1021/acsnano.7b07737.

The Surface Oxidation of Graphene Oxide Determines Membrane Damage, Lipid Peroxidation, and Cytotoxicity in Macrophages in a Pulmonary Toxicity Model

Ruibin Li[§], **Linda M. Guiney**[⫲], **Chong Hyun Chang**[⊥], **Nikhita D. Mansukhani**[⫲], **Zhaoxia Ji**[⊥], **Xiang Wang**[⊥], **Yu-Pei Liao**[†], **Wen Jiang**, **Bingbing Sun**[†], **Mark C. Hersam**[⫲], **Andre E. Nel**[†,‡,⊥,*], and **Tian Xia**[†,‡,⊥,*]

[†]Division of NanoMedicine, Department of Medicine, University of California, University of California, Los Angeles, California 90095, United States

[‡]Center for Environmental Implications of Nanotechnology, University of California, University of California, Los Angeles, California 90095, United States

[⊥]California NanoSystems Institute, University of California, University of California, Los Angeles, California 90095, United States

[#]Department of Materials Science and Engineering, University of California, University of California, Los Angeles, California 90095, United States

[⫪]Departments of Microbiology, Immunology, and Molecular Genetics, University of California, University of California, Los Angeles, California 90095, United States

[⫲]Departments of Materials Science and Engineering, Chemistry, and Medicine, Northwestern University, Evanston, Illinois 60208, United States

[§]School for Radiological and Interdisciplinary Sciences (RAD-X), Collaborative Innovation Center of Radiation Medicine of Jiangsu Higher Education Institutions, Soochow University, Suzhou, 215123, China

Abstract

While 2-dimensional graphene oxide (GO) is used increasingly in biomedical applications, there is uncertainty on how specific physicochemical properties relate to biocompatibility in mammalian systems. Although properties such as lateral size and the colloidal properties of the nanosheets are important, the specific material properties that we address here is the oxidation state and reactive surface groups on the planar surface. In this study, we used a GO library, comprised of pristine, reduced (rGO), and hydrated GO (hGO), in which quantitative assessment of the hydroxyl, carboxyl, epoxy and carbon radical contents were used to study the impact on epithelial cells and

[*]Corresponding Author: Tian Xia, Ph.D.; and Andre Nel, Ph.D., Department of Medicine, Division of NanoMedicine, UCLA School of Medicine, 52-175, CHS, 10833 Le Conte Ave, Los Angeles, CA 90095-1680. Tel: (310) 983-3359, Fax: (310) 206-8107, txia@ucla.edu, Anel@mednet.ucla.edu.

Supporting Information

Height and lateral size measurements by AFM, Confocal microscopy images of BEAS-2B cells, Cytotoxicity results at 24 hour, immunocytochemistry staining of caspase-3 and TUNEL staining in lung tissues, and LDH release in BALF. This material is available free of charge *via* the Internet at http://pubs.acs.org.

macrophages, as well as in the murine lung. Strikingly, we observed that hGO, which exhibits the highest carbon radical density, was responsible for the generation of cell death in THP-1 and BEAS-2B cells as a consequence of lipid peroxidation of the surface membrane, membrane lysis, and cell death. In contrast, pristine GO had lesser effects while rGO showed extensive cellular uptake with minimal effects on viability. In order to see how these *in vitro* effects relate to adverse outcomes in the lung, mice were exposed to GOs by oropharyngeal aspiration. Animal sacrifice after 40h demonstrated that hGO was more prone than other materials in generating acute lung inflammation, accompanied by the highest lipid peroxidation in alveolar macrophages, cytokine production (LIX, MCP-1) and LDH release in bronchoalveolar lavage fluid. Pristine GO showed less toxicity while rGO had minimal effects. In summary, we demonstrate that the surface oxidation state and carbon radical content play major roles in the induction of toxicity by GO in mammalian cells and the lung.

Graphical Abstract

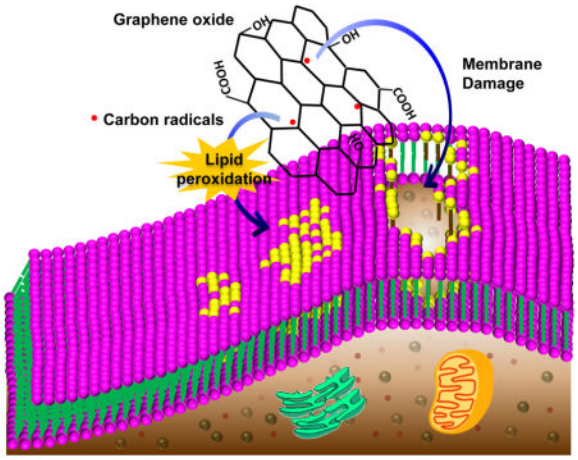

Keywords

graphene oxide; surface functional groups; structure-activity relationships; carbon radicals; lipid peroxidation; lung inflammation

---

Graphene is increasingly being used for a broad range of applications in electronics, energy, sensors, and catalysis due to its high electronic and thermal conductivity, high surface area, and extraordinary mechanical properties.[1, 2] Moreover, the graphene derivative, graphene oxide (GO), exhibits excellent dispersibility, colloidal properties and the potential to use surface functionalization to render the material attractive for use in biomedicine, including tissue engineering[3], antimicrobial agents,[4] bioimaging,[5] and drug delivery.[6] In order to be successfully translated to products that can be used in the marketplace, it is important to understand the safety and biocompatibility of GO.[7, 8] Although there has been an extensive body of work regarding the potential toxic effects of GO in bacteria, including its use for antibacterial applications,[4, 9, 10] the toxicity profile of GO in mammalian systems is still incomplete.[7, 8]

Studies looking at GO antibacterial effects have demonstrated the importance of considering the contribution of its planar 2D structure, lateral size, edges, surface functional groups and oxidation status in interactions with the bacterial membrane.[4, 9, 11–14] Theoretical simulations as well as experimental data demonstrated that the sharp corners and edge protrusions of GO enable these materials to penetrate bacterial membranes, with the possibility to extract lipid molecules and induce membrane disruption.[10] The expression of epoxy, hydroxyl, and carbon radical groups on the surface, together with carboxyl groups on the edges, contribute to bactericidal effects.[4] In contrast, a detailed understanding of how the complicated GO chemistry engages mammalian systems is still unclear and requires additional study.[4, 15,16] Among the reported effects of GO in mammalian cells is the delineation of induction of cell death.[8] For instance, studies have shown that GO could induce dose-dependent cell death in normal lung fibroblasts (HLF), macrophages (THP-1 and J744A), epithelial (BEAS-2B) cells, lung cancer cells A549, *etc.*[8] However, the data are inconsistent and even contradictory with respect to how physicochemical properties like the lateral dimentional size, surface coating (PVP, PEG, Pluronic), and oxidation states contribute to toxicological effects in mammalian systems.[8] Since GO nanosheets have also been reported to induce inflammation and fibrogenic effects in the lung,[17] we hypothesized that the oxidation status and surface reactivity of the material play a key role in these adverse outcomes, and that this organ system could be useful to delineate the structure-activity relationships related to deliberate variation of the surface properties.[4]

In order to discern the role of the oxidative modification of the GO surface in bacteria, we prepared a library of materials in which the relative abundance of the surface reactive groups was changed by catalytic chemistry.[4] One approach was solvothermal reduction to quantitatively reduce GO oxidation levels, while another was the use of hydrolysis by alkalized aqueous solvents to open the epoxy rings, thereby increasing hydroxyl and carbon radical densities.[4] This yielded a library of pristine, reduced (rGO) and hydrated GO (hGO) nanosheets that were thoroughly characterized for oxygen content, other surface groups, carbon radical content and biological oxidative potential.[4] In the current communications, a library of pristine, rGO and hGO nanosheets were prepared to delineate the effects of the surface functional groups in pulmonary epithelial cells and macrophages, as well as the murine lung. The *in vitro* experimentation was followed by oropharyngeal instillation into the murine lung, focusing on mechanistic injury responses that may explain how adverse effects at cellular level relate to an adverse outcome at organ level. We identified the critical role of surface functional groups, including carbon radicals, in impacting GO biocompatibility in the lung. This includes adverse effects on the cellular membrane, cytotoxicity, and cellular uptake, leading to pro-inflammatory effects in the lung.

Results

Preparation and characterization of GOs

To assess the biohazardous potential of key functional groups on GO, a material library was prepared by using reduction or hydration of pristine GO, as previously described (Scheme 1). Two reduced GO samples were obtained by solvothermal reduction in N-methyl-2-pyrrolidinone (NMP) for 1 h (rGO-1) and 5 h (rGO-2). Moreover, we prepared two hydrated

GO materials by suspending pristine GO in an alkalized solution at temperatures of 50°C (hGO-1) and 100°C (hGO-2), respectively. Detailed physicochemical characterization of these materials was performed. Atomic force microscopy (AFM) results show that all GO samples were composed of nanosheets with irregular shape, mostly monolayer and bilayer with height 0.8–1.6 nm and lateral dimensions of ~100–150 nm (Figure 1A, Table S1, Figure S1). Raman spectra showed the typical D and G bands representative of graphene and confirming minimal structural or through the use of reduction or hydration. These bands represent the stretching of the graphitic out-of-plane C-C bonds (D band) and in-plane G band, respectively (Figure 1B). There were no differences in the intensity ratio of the D *vs.* G bands (I_D/I_G ratio) in the various materials, which are indicative of similar ratios of sp^2 and sp^3 bonds on the GO surface.[18] Please note that Raman I_D/I_G ratios provide a general indication of the abundance of the level of graphene surface defects, which include oxygen containing surface as well as structural defects. Although the reduction process for rGOs lowered the number of oxygen-containing defects, the process could generate hexagonal point defects resulting from the addition or removal of carbon atoms on the GO surface. Consequently, the overall surface defect levels remain approximately similar across samples. Due to the intended material use in cellular studies, we also assessed the hydrodynamic size and zeta potential of the materials in deionized water (DI H_2O) and the tissue culture media (Table 1). Most GO samples showed agglomeration in DI H_2O, resulting in hydrodynamic diameters of 330–440 nm, except for rGO-2 that showed larger (550 nm) agglomerates as a result of reduced hydrophilicity. All GO samples showed hydrodynamic diameter sizes of 320–460 nm in RPMI 1640 medium compared to a size range of 550–600 nm in BEGM medium; the reduced size in the former medium is due to the presence of a high concentration of serum albumin, which leads to the formation of a protein corona.[19, 20]

We also performed extensive characterization of the surface functional groups. X-ray photoelectron spectroscopy (XPS) was used to characterize the oxygen functional groups. As shown in Table 2, the reduction of GO to rGO-2 was accompanied by a significant decrease in oxygen-containing moieties. The atomic percentages of total oxygen, C-OH, C=O and C-O-C decreased from 36.7 to 16.5%, 6.8 to 4.1%, 9.4 to 8.3%, and 20.5 to 4.1%, respectively. During the hydration process, epoxy rings react with nucleophiles in aqueous solution, generating C-OH groups and carbon radicals[4] (Figure 1C). We used electron paramagnetic resonance (EPR) to assess the presence of surface carbon radicals (•C), as demonstrated in Figure 1C. GO samples that contain p-conjugated carbon radicals, showed EPR peaks at g= 2.0029.[4] For rGO-2, the •C peak intensity is reduced from 1.85×10^5 for pristine GO to extremely low level (0.01×10^5) (Table 2). In contrast, the hydration reaction increases carbon radical density (8.38×10^5 for hGO-2), accompanied by a decrease in C-O-C and an increase in C-OH groups (Table 2, Figure 1C). Carbon radicals are typically considered more reactive than other surface functionalities due to the presence of unpaired electrons. These electrons are capable of reacting with molecular dioxygen to generate superoxide radicals, which are capable of oxidizing unsaturated lipids and thiol groups on proteins or glutathione (GSH) (Figure 1C).[21] GSH also plays a major role in maintaining redox equilibrium in cells, whether ratio of reduced to oxidized glutathione (GSSG) is important in cellular homeostasis, with the potential to trigger a series of hierarchical oxidative stress responses.[22–25] Thus, we chose GSH as a model system to test the pro-

oxidative potential of GO, using an abiotic GSH-Glo™ assay (Figure 1D). While hGO-2 could deplete GSH by 96%, the respective values for pristine GO and rGO-2 were 80% and 16%, respectively. In summary, there is good agreement between the carbon radical density on the GO surface, the degree of pro-oxidant activity and the extent of GSH depletion.[4]

Plasma membrane association and cellular uptake of GO

Cellular responses to GO are dependent on physical interactions with the plasma membrane, following which there is the possibility of cellular uptake and the potential to interact with subcellular structures.[8] Previous studies have demonstrated that the lateral GO flake size may determine cellular interactions to the extent that a large lateral size may restrict the ability to be taken up by cells.[17] In accordance with this view, smaller GO flakes were more readily taken up into the cell without significant interaction with the plasma membrane.[17] The study did not take into consideration the impact of surface functionality and the oxidation status of GO. To clarify this point, THP-1 cells were incubated with pristine, reduced and hydrated GO samples for 16 h, before TEM analysis (Figure 2A). And limitation of this technique is that the low electron density of GO, only allows visualization of the suspended GO when vertically positioned but for nanosheets that are horizontally aligned with the grid. Nonetheless, in spite of the shortcoming it was possible to demonstrate that GO or hGO-2 nanosheets insert or attach to the surface membrane of THP-1 cells (Figure 2A). This interaction with the mammalian cell lipid bilayer is likely premised on the amphiphilic nature of these materials, which display a hydrophobic planar structure with hydrophilic edges.[26] In contrast, rGO-2 has a reduced number of hydrophilic edge groups, is more hydrophobic in nature and is principally internalized by phagocytic uptake in THP-1 cells. The TEM observations were further substantiated by visualizing the cellular processing of FITC-BSA labeled GO samples in THP-1 (Figure 2B) and BEAS-2B cells (Figure S2). Confocal microscopy demonstrated that while hGO and GO showed extensive accumulation in proximity to the surface membrane, without much cellular uptake, rGO did not localize at the surface membrane and could be visualized inside cells.

Pristine and hGO induce lipid peroxidation of the surface membrane

Since pristine GO and hGO-2 are capable of GSH depletion (Figure 1D), we were interested to see if this leads to lipid peroxidation during the accumulation of these materials at the surface membrane. Lipid peroxidation was studied by using the BODIPY® 581/591 C11 reagent to visualize the green shift (~510 nm) in fluorescence activity (from red at ~590 nm) in the presence of lipid peroxides. As shown in the confocal microscopy images in Figure 3A, cumene hydroperoxide (CH), used as a positive control reagent, induced a substantial switch to green fluorescence at the expense of the red fluorescence in the plasma membrane of THP-1 cells. While pristine GO also the ship to faint red fluorescence, hGO-2 had a pronounced effect, while the effect of rGO-2 was limited. The data was also quantitatively expressed by conducting flow cytometry and calculating the percentage of cells exhibiting increased fluorescence intensity at 510 nm (Figure 3B). This showed that relative abundance of lipid peroxidation in THP-1 amounts to 13, 37 and 5% of cells in the population in response to pristine GO, hGO-2 and rGO-2, respectively.

Lipid peroxidation can lead to a failure in membrane integrity. Direct evidence of membrane damage was provided by using a hemolysis assay in red blood cells (RBC). RBC lack fluid phase or receptor- mediated endocytosis, and is widely used to study nanomaterial interactions with the membrane.[27, 28] While the hemolysis assay demonstrated little or no RBC lysis during rGO-2 treatment, pristine GO showed dose-dependent hemolysis, which amounted to 20% of cells being lysed at 200 Sg/ml (Figure 3C). In contrast, the hemolytic potential of hGO-2 amounted to 68% of RBCs lysed at 50 Sg/ml (Figure 3C). Please notice that the apparent decrease in the % hemolysis at GO doses >50 ug/ml is likely due to adsorption of released hemoglobin onto the GO surface. These results are in good agreement with the change in membrane peroxidation.

Induction of Cytotoxicity by GO Nanosheets

Because lipid peroxidation can trigger cell death, we evaluated the cytotoxic potential GO nanosheets in THP-1 and BEAS-2B cells. After 48 h exposure most GO samples show significant cytotoxicity in THP-1 and BEAS-2B cells in the ranking order: hGO-2 > hGO-1 > GO > rGO-1 > rGO-2 (Figure 4A). Interestingly BEAS-2B cells were more sensitive to the cytotoxic effects of hGO than THP-1 cells. These effects are time-dependent, as demonstrated by the fact that only hGO-2 shows toxicity in THP-1 cells after 24 h of exposure (Figure S3). The cytotoxicity ranking of the various types of GO correlates well with the carbon radical density, yielding correlation coefficients of 0.95 in BEAS-2B cells and 0.98 in THP-1 cells (Figure 4B). These data confirm the importance of carbon radicals on the GO in promoting toxicity in mammalian cells. Heat maps were used to integrate the data sets for lipid peroxidation, membrane leakage and cell death, using a one-way ANOVA statistical method (Figure 4D). Visual data display, where red indicates significant toxicity and green represents absence of toxicity, demonstrates excellent correlation among the cellular response parameters, confirming a hazard ranking of hGO-2 > hGO-1 > GO > rGO-1 > rGO-2. While hGO-2 induces significantly higher toxicity than pristine GO, rGO-2 had the least hazardous potential.

Induction of acute lung inflammation by GO nanosheets

To see if the *in vitro* hazard profiling is predictive of *in vivo* toxicological outcome, we used an oropharyngeal aspiration approach, according to which mice were exposed to 2 mg/kg hGO-2, GO, and rGO-2. This dose was selected based on prior dose-response studies, where a dose of 2 mg/kg for graphene and GO falls on the linear part of the dose response curve.[17] Following exposure for 40 h, animals were sacrificed and bronchoalveolar lavage fluid (BALF) obtained to examine the effects of GO on cells and cytokines. Raman microscopy was used to assess GO uptake in pulmonary macrophages (Figure 5A). Characteristics D and G bands were obtained for all GO materials, demonstrating that GO and hGO-2 are largely associated with the cell membrane, while rGO-2 was taken up into the cell. These results are with the cellular TEM and confocal data (Figure 2). We also demonstrated the presence of lipid peroxidation in alveolar macrophages, by using Image-iT® lipid peroxidation kit for confocal viewing (Figure 5B). This demonstrated that the % of cells undergoing lipid peroxidation (green fluorescence) amounted to 69% and 55% in animals exposed to GO and hGO-2, respectively (Figure 5C). Quartz was used as a positive control and resulted in lipid peroxidation in 50% of the cells. In contrast, the percent lipid peroxidation was 11% in the

BALF cells of rGO-2 exposed animals. We also assessed permeability of the BALF cells, using propidium iodide (PI) staining.[29] As demonstrated in Figure 5D, BAL cells from hGO-2 exposed animals showed ~ 40% PI-positive cells, 22% for GO and 5% for rGO-2. These data show that the impact of the GO-materials on pulmonary alveolar macrophages duplicate the results seen in tissue culture cells.

We also assessed pro-inflammatory effects in the lung. Quartz and hGO-2 induced significantly higher levels of neutrophil recruitment to the BALF, compared to exposure to pristine GO and rGO-2 (Figure 6A). The pro-inflammatory response in the BALF was also reflected in the intensity of focal pulmonary infiltrates, as demonstrated by hematoxylin and eosin (H&E) staining (Figure 6B). Moreover, GO and hGO also induced significantly higher levels of the pro-inflammatory cytokines, LIX and MCP-1, in the BALF (Figure 6C). Assessment of lung cell death by TUNEL staining or immunohistochemistry analysis of the expression of activated caspase-3, showed significantly more cytotoxicity in the lungs of animals exposed to GO and hGO compared to rGO (Figure S4A and S4B), Pulmonary cytotoxicity was further confirmed by assessment of lactate dehydrogenase (LDH) release in the BALF, which confirmed higher levels in GO and hGO exposed animals than mice aspirating rGO (Figure S5).

Discussion

In this study, we used a GO library with different GO surface functionalities to determine the hazard potential in pulmonary cell types and the lung. We demonstrated that pristine GO and hydrated GO samples, which express the highest •C densities, exhibit the highest pro-oxidative effects *in vitro* and *in vivo*, as evidenced by the tracking of lipid peroxidation, membrane leakage and cell death, compared to reduced GO. The *in vitro* results were confirmed in mice exposed to GO by oropharyngeal aspiration. GO and hGO-2 induce significantly higher BALF cell counts, production of pro-inflammatory cytokines (including MCP-1 and LIX), lipid peroxidation in macrophage membranes and death of the cells than rGO. Moreover, these pro-inflammatory effects were also duplicated in the appearance of pulmonary infiltrates in the lung and *in situ* staining for cytotoxicity. Collectively, these data demonstrate that the *in vitro* and *in vivo* hazard potential of GO is determined, in part, by low surface functionalization, in particular, the density of •C on the material surfaces. This information is considerable importance in understanding the hazard potential of GO in mammalian tissues, and provide structure-activity relationships that can be used for safer designed materials.

The most significant finding in this communication is that the level of oxidative modification of the GO surface as well as the presence of carbon radicals determine the *in vitro* and *in vivo* hazard potential, as reflected by lipid peroxidation of the surface membrane, membrane damage, subcellular processing, cytotoxicity, and the generation of acute pro-inflammatory effects in small airways of the lung. This indicates that the structure-activity relationships related to the oxidation status and expression of surface OH, COOH, COC groups and carbon radicals, needs to be included with physicochemical properties such as edge size and colloidal behavior, which depends on the relative degree of hydrophobicity of the planar surface and charged edges.[15,19] In light of the limited variation of GO nanosheet thickness

(number of layers) and lateral size dimensions in this study, the strongest correlation to cytotoxicity was the oxidation status and carbon radical density of our GO nanosheets. Collectively, these properties determine the hazard potential of GO, which can dynamically differ from material to material.[8, 30] This complexity may also explain the apparent discrepancies in the data on GO toxicity, which could vary as a result of the experimental approach and different exposure routes.[8, 17, 30] While some *in vitro* and *in vivo* studies clearly show that GO pose no particular risks and can be of beneficial biological use,[31–34] others have indicated that GO nanosheets can be hazardous.[17] Recently, Jasim *et al.* found that GO exhibited negligible liver and renal toxicity following intravenous injection of GO in mice, at doses up to 10 mg/kg.[34] However, this stands in contrast to studies showing that intravenously injected GO could induce significant inflammation and fibrosis in the liver or kidney.[35–37] It has also been shown that GO could provoke fibrogenic effects in the lungs following oropharyngeal aspiration.[17, 38] Moreover, the pulmonary effects are dependent on the GO surface functionalities and can be reduced by Pluronic coating.[17] Sydlik *et al.* have also suggested that the oxidation level of GO may determine its toxicity.[30] However, due to the complexity of the surface functional groups, including the presence of •C, it is unclear what the role of each functionality is in terms of potential hazardous impact.[4] Through the establishment of a well-characterized GO library that systematically varied the level of surface expression, we demonstrate that the most proximate indicator of pulmonary toxicity is correlated to the surface •C densities. Hydration enhances density and expression of these radicals by opening the epoxy groups on GO surface.[4] Reduction has the opposite effect. The carbon radicals are embedded in the p-network plane, allowing single unconjugated electrons to associate with the electronic structure of the neighboring double bonds, and ability to travel through the linked C=C network.[4] Thus, the entire GO nanosheet could function as “super porphyrin” structure with embedded carbon radicals.[39] With the ability of •C to donate electrons resulting in the formation of the superoxide radical, it is possible that unsaturated lipids in contact with the GO basal plane can be oxidized, leading to the formation of lipoperoxides.[4]

Another interesting aspect of our study relates to the different sites of cellular localization of pristine, hydrated and reduced GO. While most GO and hGO nanosheets associated with the surface membrane in THP-1 and BEAS-2B cells, rGO was principally taken up into the cell. These results are in agreement with the data of Mari *et al.*, who demonstrated that while large amounts of GO could be seen to be located principally in the plasma membrane, graphene was taken up into the cytoplasm of a neuroblastoid cell line, SK-N-BE(2).[40] The differences we observed may depend on differences in the amphiphilic properties of the materials. Thus, while GO and hGO exhibit hydrophilic edges and hydrophobic planar surfaces that may affect membrane association, the hydrophobicity of the rGO nanosheets may be involved in increased propensity for cellular uptake. The issue is complicated, however, because some reports show that pristine GO could be internalized into the cytoplasm.[41–43] Could this be due to differences between cell types (*e.g.*, phagocytic *versus* non-phagocytic cells or different stages of cell differentiation) or is the cellular association principally determined by physicochemical properties? Mu *et al.* reported a size-dependent contribution to cellular uptake of GO nanosheets that exhibit a protein corona.[41] Their study suggested that small GO sheets are taken up principally by clathrin-mediated endocytosis

while larger sheets are internalized by a process of phagocytosis.[41] This stands in contrast with the work of Ma *et al.*, who showed that the majority of BSA-FITC-labeled GO nanosheets of the larger size were associated with the cell membrane while small GO sheets were internalized by the macrophage cell line, J774A.1.[17] These are not the only parameters, however, that determine cellular uptake, and one also have to consider the impact of GO surface charge and functionalization, similar to what we show.[44] This complexity can only be addressed by considering a further extension of the combinatorial library concept, where in addition to control over the surface functionality, one would also introduce additional parameters and other cell types to reach a final conclusion.

Our study focused on the pulmonary toxicity because some GOs are prepared in powder form and used in applications such as coatings, conductive inks or paints, additives in polymeric composites or absorbents, which can readily be aerosolized and inhaled.[45, 46] However, GO has been explored for use in medical devices, tissue engineering, and drug delivery, which introduces additional exposure scenarios and potential risks.[30] Langer *et al.* have shown that GO is moderately biocompatible at the subcutaneous and intraperitoneal injection sites, where an inflammatory reaction may develop.[30] Chemical reduction of GO resulted in accelerated immune cell infiltration, uptake, and clearance at these injection sites.[30] In another study, it was demonstrated that GO-coated substrates could significantly enhance the differentiation of mouse embryonic stem (ES) cells to both primitive and differentiated hematopoietic cells.[47] All considered, the collective body of work would seem to suggest that differences in GO usage could change the exposure scenarios and types of tissues and organs that could be impacted. The responses in the lung are not necessarily indicative of effects elsewhere. Our study demonstrates the importance of considering all the variables at play in contemplating the use of GO for biological experimentation or assessment of its potential adverse health effects for different exposure scenarios.

Conclusions

In this study, we prepared a library of GO nanomaterials with different levels of surface functionalities to explore the potential to induce acute lung inflammation. Carbon radicals were found to be the dominant surface functionality that induces cytotoxicity in THP-1 and BEAS-2B cells. This toxicity pathway involves plasma membrane adsorption, lipid peroxidation, membrane damage, and cell death. These *in vitro* toxicological pathways are also responsible for acute inflammation in the murine lung following local exposure. hGO-2, representative of a material with high carbon radical density, induced significantly more lipid peroxidation and membrane damage in tissue culture cells than rGO. These results also accurately predict similar effects in primary alveolar macrophages, along with inducing acute pro-inflammatory responses in the lung. Pristine GO showed moderate effects, while rGO-2 induced low levels of lung inflammation. The study provides valuable information on how to structure the toxicological profiling of GO nanosheets exhibiting different levels of surface functionality.

Materials and Methods

Chemicals

The Beta-Glo® Assay System, CytoTox 96® Non-Radioactive Cytotoxicity Assay, GSH-Glo™ Glutathione Assay, CellTiter-Glo® Luminescent Cell Viability Assay (ATP) and CellTiter 96® AQueous One Solution Cell Proliferation Assay (MTS) were purchased from Promega (Madison, WI, USA); graphite flakes were provided by Asbury Graphite Mills; Hoechst 33342, FITC labeled Bovine Serum Albumin (BSA), Alexa Fluor 594-conjugated wheat germ agglutinin (WGA), Propidium iodide and Image-iT® Lipid Peroxidation Kit were purchased from Life Technologies (Grand Island, NY, USA). Min-U-Sil was obtained from U.S. Silica (Frederick, MD, USA). Bronchial epithelial growth medium (BEGM) was obtained from Lonza (Mapleton, IL, USA): this medium is supplemented with a number of growth factors, including bovine pituitary extract (BPE), insulin, hydrocortisone, hEGF, epinephrine, triiodothyronine, transferrin, gentamicin/amphotericin-B and retinoic acid. Roswell Park Memorial Institute medium 1640 (RPMI 1640) was purchased from Invitrogen (Carlsbad, CA, USA). Low-endotoxin bovine serum albumin (BSA) and fetal bovine serum (FBS) were purchased from Gemini Bio-Products (West Sacramento, CA, USA).

Acquisition and synthesis of a surface functionalized GO library

The GO library was established using methods reported previously.[4] Pristine GO was prepared by a modified Hummers' method. We performed ICP-MS to determine the level of impurities and the results showed that all elements including metal impurities are negligible level (<0.04 wt. %) (data not shown). To prepare reduced GO, pristine GO was dispersed in NMP by ultrasonication for 1 h at 50% power (~55 W). The solution was heated to 150 °C with constant stirring in a silicone oil bath for 1 hour (rGO-1) or 5 h (rGO-2). For the preparation of hydrated GO, 10 mL pristine GO suspension (5 mg/mL) was diluted with 90 mL deionized (DI) water and mixed with 80 mg NaOH (0.02 M), using dispersal by a sonication probe (Sonics & Materials, USA) at 32 W for 10 s. The GO mixture was transferred into a round flask and refluxed at 50 or 100 °C in an oil bath with constant magnetic stirring for 24 h. 1 M HCl solutions were used to neutralize the reaction. The mixture was centrifuged at 50,000 rpm for 30 min to collect the hydrated GO pellets. After washing with DI water three times, the hydrated GO samples were dispersed in DI water and stored at 4 °C.

Physicochemical characterization of GO samples

To obtain AFM images, Si wafers were pretreated by 2.5 mM (3-aminopropyl) triethoxysilane (APTES) aqueous solution for 30 min to functionalize the surface with a monolayer. The wafers were rinsed twice with DI water and dried under N_2. A drop of 10 μg/mL GO solution was placed on the wafer, followed by washing twice with DI water (~5 s) and drying under N_2. The GO sample then underwent heat treatment for 30 min at 250°C. AFM images were obtained by an Asylum Research Cypher ES AFM. Images were taken at random locations on the sample and showed little variation. All images were obtained with the same tip and scanning conditions.

X-ray photoelectron spectroscopy (XPS, AXIS Ultra DLD, Kratos, UK) has been used to investigate the chemical state and calculate the atomic concentration of oxidized groups on the GO surface with monochromatic Al Ka at 15 kV and 10 mA. For sample preparation, suspensions of GO samples were dropped on the silicon substrate and dried at room temperature. The data analysis and curve fitting were performed with the CasaXPS program (Casa Software Ltd., UK).

The molecular structure of all GO samples was characterized using Raman spectroscopy (Renishaw in *Via* Reflex, Wotton under Edge, UK) with a 785 nm near-infrared diode and a 50X objective lens. Spectra were obtained using 10 seconds exposure to obtain two scans 1000–2000 cm^{-1} in the wave number region.

The EPR measurements were obtained with an X-band Bruker ELEXYS 580 spectrometer. 5 mg GO nanosheets were dried under vacuum, and allowed to settle on the bottom of 2 mm ID quartz EPR tubes prior to data collection. The field was calibrated using a standard sample with a known *g*-factor (2,2-diphenyl-1-picrylhydrazyl, DPPH). The EPR spectra were detected at room temperature with frequency at 9.785845 GHz, center field at 3480 G, attenuator at 13.0 dB and g value at 2.0029.

Zeta-potential and hydrodynamic size measurements of the GO suspensions were performed using a ZetaSizer Nano-ZS instrument (Malvern Instruments, Worcestershire WR, UK).

Assessing the pro-oxidative potential of GO, using a GSH assay

Assessment of the GSH content was obtained by using a GSH-Glo™ Glutathione Assay.[48] This is a luminescence-based assay for detecting and quantifying glutathione (GSH). The assay is based on the conversion of a luciferin derivative to luciferin by glutathione S-transferase (GST). The signal generated in a coupled reaction with firefly luciferase is proportional to the amount of glutathione present in the sample. The assay was performed under abiotic conditions by adding 10 μL aliquots of Co_3O_4 or GO at 5 mg/mL to a 96-well plate together with 90 μL GSH-Glo agent for 30 min. The luciferin detection agent was added to each well (100 μL/well) and the luminescence was detected by on a SpectraMax M5 microplate spectrophotometer (Molecular Devices, Sunnyvale, CA).

Assessment of cellular viability by a MTS assay

BEAS-2B and THP-1 cells were obtained from ATCC (Manassas, VA), and cultured were cultured in BEGM or complete RPMI 1640 (supplemented with 10 % fetal bovine serum), respectively, at 5 % CO_2 and 37°C. Before exposure to GO samples, BEAS-2B cells were seeded at a density of 1×10^4/well in 96-well plates (Corning, NY, USA) overnight at 37°C. All the GO solutions were freshly prepared in BEGM containing 0.2% BSA or in complete RPMI 1640. These suspensions were dispersed by sonication (Sonics & Materials, USA) at 32 W for 10 s at the desired final concentration, before addition to the cells. Aliquots of 3×10^4 THP-1 cells were seeded overnight in 0.1 mL complete RPMI medium into 96-well plates (Corning, NY, USA), receiving 1 Sg/mL phorbol 12-myristate acetate (PMA), while BEAS-2B cells were suspended in BEGM media at a density at 1×10^4 cells per well. After exposure to 0–200 μg/mL of each of the GO suspensions for 24 or 48 h, the cell culture medium was removed, followed by the addition of 120 μL culture medium containing 10%

MTS stock solution for 1–2 hour at 37 °C in a humidified 5% CO_2 incubator.[27] The supernatants were transferred to a 96-multiwell plate and centrifuged at 2000g for 10 min in NI Eppendorf 5430 to spin down the cell debris and nanoparticles. 100 μL of the supernatant was removed from each well and transferred into a 96-well plate. The absorbance of formed formazan was read at 490 nm on a SpectraMax M5 microplate spectrophotometer.

Confocal imaging of BSA-FITC labeled GO samples in cells

BSA-FITC labeled GO samples were prepared by a diimide-activated amidation reaction as described before.[49] Briefly, 5 mg EDC and 10 mg NHS were dissolved in 2 mL rGO-2, GO or hGO-2 suspensions (100 μg/mL) in water and the mixtures stirred for 2 hr at room temperature. The GO pellets were collected by centrifugation at 20,000 rpm for 10 min, and reacted with 1 mL of a suspension containing 0.1 mg/mL of the BSA-FITC solution while stirring for 2 h. The FITC labeled GO samples were collected by centrifugation at 20,000 rpm for 10 min, suspended in 400 μL DI water and stored at 4 °C for further use. For confocal imaging, 300 μL aliquots of THP-1 and BEAS-2B cell suspensions, at densities at 3×10^5/mL and 1×10^5/mL, respectively, were seeded into 8 well chambers (Nunc® Lab-Tek® II chambered coverglass, Sigma-Aldrich) for overnight incubation. The cells were exposed to 25 μg/mL of the various GO suspensions for 16 h, followed by 5 washes in PBS. Cell membranes and nuclei were stained with Alexa Fluor 594-conjugated WGA and Hoechst 33342, respectively, at room temperature for 1 h. The cells were visualized under a confocal microscope (Leica Confocal SP2 1P/FCS). High magnification images were obtained under the 63X objective.

Assessment of cell membrane lipid peroxidation

THP-1 cells were treated with 100 μg/mL of each of the GO samples for 16 h or 10 μM cumene hydroperoxide (positive control) for 1 h. Aveolar macrophages were obtained from the BALF of mice exposed to 5 mg/kg quartz or 2 mg/kg rGO-2, GO or hGO-2 for 40 h, and allowed to adhere to the bottom of 8-well chambers. After washing, the cells were incubated with 10 SM Image-iT® Lipid Peroxidation Sensor and Hoechst 33342 in culture media for 30 min.[4]. The stained cells were washed three times in PBS, and used for confocal microscopy under a TCSSP2 confocal laser scanning microscope (Leica, Wetzlar, Germany) for visualization of the reduced and oxidized fluorescent dye at excitation/emission wavelengths of 581/591 nm (Texas Red® filter set) and 488/510 nm (traditional FITC filter), respectively. We also performed flow cytometry analysis on a FACS Vantage SE flow cytometer from BD (Franklin Lakes, NJ), using FlowJo® Software (Ashland, OR) to calculate the ratio of the emission fluorescence intensities at 590 nm to 510 nm.

RBC hemolysis assay

Heparinized mouse blood was washed with saline, following which the RBCs were diluted to 1×10^8 cell/mL in PBS. 490 μL of the diluted RBC suspension was mixed with 10 μL of GO nanoparticles to achieve final concentrations of 0–200 μg/ml. The addition of saline was used as a negative control while 0.25% Triton X-100, served as positive control. The mixtures were gently stirred and incubated for 3 h at 37ºC. The samples were centrifuged and the absorbance of the supernatants measured at 541 nm in a SpectraMax M5 microplate

spectrophotometer. The percent hemolysis in each sample was calculated as previously described.[27]

Use of TEM to detect of cellular uptake of GO

After exposure to 100 μg/mL rGO-2, GO or hGO-2 for 16 h, the cells were washed and fixed with 2% glutaraldehyde in PBS. Following post-fixation in 1% osmium tetroxide in PBS for 1 h, the cells were dehydrated in a graded series of ethanol, and then treated with propylene oxide before embedding in Epon. Approximately 50–70 nm thick sections were cut on a Reichert-Jung Ultracut E ultramicrotome and picked up on Formvar-coated copper grids. The sections were stained with uranyl acetate and Reynolds lead citrate and examined on a JEOL transmission electron microscope at 80 kV in the UCLA BRI Electron Microscopy Core, as previously reported.

Animal treatment and assessment of exposure outcomes

Eight-week-old male C57Bl/6 mice purchased from Charles River Laboratories (Hollister, CA) were used for exposure studies. All animals were housed under standard laboratory conditions according to UCLA guidelines for care and treatment of laboratory animals as well as conforming to the NIH Guide for the Care and Use of Laboratory Animals in Research (DHEW78-23). These conditions are approved by the Chancellor's Animal Research Committee at UCLA and include standard operating procedures for animal housing (filter-topped cages; room temperature at 23 ± 2 °C; 60% relative humidity; 12 h light, 12 h dark cycle) and hygiene status (autoclaved food and acidified water). Animal exposure to GO materials was carried out by an oropharyngeal aspiration method as described by us.[50] Animals were anesthetized by intraperitoneal injection of ketamine (100 mg/kg)/xylazine (10 mg/kg) in a volume of 100 μL. The animals being held in a vertical position, 50 μL aliquots, containing 2 mg/kg of each of the GO suspensions in PBS plus 0.6 mg/mL BSA and 0.01 mg/mL DPPC, were instilled at the back of the tongue for pulmonary aspiration. Control animals received the same volume of PBS. The positive control group in each experiment received 5 mg/kg quartz particles (Min-U-Sil). The mice were sacrificed after 40 h exposure. BALF and lung tissue were collected as previously described. The BALF was used for performance of total and differential cell counts and measurement of LIX and MCP-1 levels. Lung tissue was stained with hematoxylin/eosin, or used for TUNEL staining or used for immunohistochemistry (ICC) analysis of activated caspase 3.

Confocal Raman microscopy

Raman analysis was performed using backscattering geometry in a confocal configuration at room temperature in a Renishaw in *Via* Raman microscope system, equipped with a 514.5 nm Ar laser.[50] Laser power and beam size were approximately 2.5 mW and 1 μm, respectively, while the integration time was adjusted to 15 s. Primary alveolar macrophages obtained from the BALF of sacrificed animals, were suspended in c-RPMI 1640 medium and seeded onto sterile glass cover slips. After 2 h incubation, cells were washed, fixed in 4 % paraformaldehyde and examined under the Raman microscope.

Statistical Analysis

Mean and standard deviation (SD) were calculated for each parameter. Results were expressed as mean ± SD of multiple determinations. Comparisons between groups were evaluated by two-side Student's t-test or one-way ANOVA. A statistically significant difference was assumed with p was < 0.05.

Supplementary Material

Refer to Web version on PubMed Central for supplementary material.

Acknowledgments

Research reported in this publication was supported by the National Institute of Environmental Health Sciences of the National Institutes of Health under Award Number R01 ES022698. Infrastructure support was also provided by the National Science Foundation and the Environmental Protection Agency under Award No. DBI-1266377. RL is supported by a grant from the National Natural Science Foundation of China (No. 31671032), and a project funded by the Priority Academic Program Development of Jiangsu Higher Education Institutions (PAPD).

References

1. Chen D, Feng H, Li J. Graphene Oxide: Preparation, Functionalization, and Electrochemical Applications. Chem Rev. 2012; 112:6027–6053. [PubMed: 22889102]
2. Compton OC, Nguyen ST. Graphene Oxide, Highly Reduced Graphene Oxide, and Graphene: Versatile Building Blocks for Carbon-Based Materials. Small. 2010; 6:711–723. [PubMed: 20225186]
3. Akhavan O, Ghaderi E, Shirazian SA, Rahighi R. Rolled Graphene Oxide Foams as Three-Dimensional Scaffolds for Growth of Neural Fibers Using Electrical Stimulation of Stem Cells. Carbon. 2016; 97:71–77.
4. Li R, Mansukhani ND, Guiney LM, Ji Z, Zhao Y, Chang CH, French CT, Miller JF, Hersam MC, Nel AE, Xia T. Identification and Optimization of Carbon Radicals on Hydrated Graphene Oxide for Ubiquitous Antibacterial Coatings. ACS Nano. 2016; 10:10966–10980. [PubMed: 28024366]
5. Zheng XT, Ananthanarayanan A, Luo KQ, Chen P. Glowing Graphene Quantum Dots and Carbon Dots: Properties, Syntheses, and Biological Applications. Small. 2015; 11:1620–1636. [PubMed: 25521301]
6. Chen Y, Tan C, Zhang H, Wang L. Two-Dimensional Graphene Analogues for Biomedical Applications. Chem Soc Rev. 2015; 44:2681–2701. [PubMed: 25519856]
7. Sydlik SA, Jhunjhunwala S, Webber MJ, Anderson DG, Langer R. *In Vivo* Compatibility of Graphene Oxide with Differing Oxidation States. ACS Nano. 9:3866–3874. [PubMed: 25849074]
8. Zhang B, Wei P, Zhou Z, Wei T. Interactions of Graphene with Mammalian Cells: Molecular Mechanisms and Biomedical Insights. Adv Drug Deliv Rev. 2016; 105:145–162. [PubMed: 27569910]
9. Akhavan O, Ghaderi E. Toxicity of Graphene and Graphene Oxide Nanowalls against Bacteria. ACS Nano. 2010; 4:5731–5736. [PubMed: 20925398]
10. Li Y, Yuan H, von dem Bussche A, Creighton M, Hurt RH, Kane AB, Gao H. Graphene Microsheets Enter Cells through Spontaneous Membrane Penetration at Edge Asperities and Corner Sites. Proc Natl Acad Sci U S A. 2013; 110:12295–12300. [PubMed: 23840061]
11. Azimi S, Behin J, Abiri R, Rajabi L, Derakhshan AA, Karimnezhad H. Synthesis, Characterization and Antibacterial Activity of Chlorophyllin Functionalized Graphene Oxide Nanostructures. Sci Adv Mater. 2014; 6:1–11.
12. Yang K, Ma YQ. Computer Simulation of the Translocation of Nanoparticles with Different Shapes across a Lipid Bilayer. Nat Nanotechnol. 2010; 5:579–583. [PubMed: 20657599]
13. Chen J, Wang X, Han H. A New Function of Graphene Oxide Emerges: Inactivating Phytopathogenic Bacterium Xanthomonas Oryzae Pv. Oryzae. J Nanopart Res. 2013; 15:1658.

14. Pham VTH, Truong VK, Quinn MDJ, Notley SM, Guo YC, Baulin VA, Al Kobaisi M, Crawford RJ, Ivanova EP. Graphene Induces Formation of Pores That Kill Spherical and Rod-Shaped Bacteria. ACS Nano. 2015; 9:8458–8467. [PubMed: 26166486]
15. Hu WB, Peng C, Luo WJ, Lv M, Li XM, Li D, Huang Q, Fan CH. Graphene-Based Antibacterial Paper. ACS Nano. 2010; 4:4317–4323. [PubMed: 20593851]
16. Liu SB, Zeng TH, Hofmann M, Burcombe E, Wei J, Jiang RR, Kong J, Chen Y. Antibacterial Activity of Graphite, Graphite Oxide, Graphene Oxide, and Reduced Graphene Oxide: Membrane and Oxidative Stress. ACS Nano. 2011; 5:6971–6980. [PubMed: 21851105]
17. Ma J, Liu R, Wang X, Liu Q, Chen Y, Valle RP, Zuo YY, Xia T, Liu S. Crucial Role of Lateral Size for Graphene Oxide in Activating Macrophages and Stimulating Pro-Inflammatory Responses in Cells and Animals. ACS Nano. 2015; 9:10498–10515. [PubMed: 26389709]
18. Grimm S, Schweiger M, Eigler S, Zaumseil J. High-Quality Reduced Graphene Oxide by Cvd-Assisted Annealing. J Phys Chem C. 2016; 120:3036–3041.
19. Ji Z, Jin X, George S, Xia T, Meng H, Wang X, Suarez E, Zhang H, Hoek EMV, Godwin H, Nel AE, Zink JI. Dispersion and Stability Optimization of Tio2 Nanoparticles in Cell Culture Media. Environ Sci Technol. 2010; 44:7309–7314. [PubMed: 20536146]
20. Koh WL, Tham PH, Yu H, Leo HL, Kah JCY. Aggregation and Protein Corona Formation on Gold Nanoparticles Affect Viability and Liver Functions of Primary Rat Hepatocytes. Nanomedicine. 2016; 11:2275–2287. [PubMed: 27527273]
21. Zhao Y, Jafvert CT. Environmental Photochemistry of Single Layered Graphene Oxide in Water. Environ –Sci Nano. 2015; 2:136–142.
22. Xia T, Zhu Y, Mu L, Zhang ZF, Liu S. Pulmonary Diseases Induced by Ambient Ultrafine and Engineered Nanoparticles in Twenty-First Century. Natl Sci Rev. 2016; 3:416–429. [PubMed: 28649460]
23. Nel AE, Maedler L, Velegol D, Xia T, Hoek EMV, Somasundaran P, Klaessig F, Castranova V, Thompson M. Understanding Biophysicochemical Interactions at the Nano-Bio Interface. Nat Mater. 2009; 8:543–557. [PubMed: 19525947]
24. Nel A, Xia T, Meng H, Wang X, Lin SJ, Ji ZX, Zhang HY. Nanomaterial Toxicity Testing in the 21st Century: Use of a Predictive Toxicological Approach and High-Throughput Screening. Accounts Chem Res. 2013; 46:607–621.
25. Nel A, Xia T, Madler L, Li N. Toxic Potential of Materials at the Nanolevel. Science. 2006; 311:622–627. [PubMed: 16456071]
26. Kim J, Cote LJ, Kim F, Yuan W, Shull KR, Huang JX. Graphene Oxide Sheets at Interfaces. J Am Chem Soc. 2010; 132:8180–8186. [PubMed: 20527938]
27. Li R, Ji Z, Chang CH, Dunphy DR, Cai X, Meng H, Zhang H, Sun B, Wang X, Dong J, Lin S, Wang M, Liao YP, Brinker CJ, Nel A, Xia T. Surface Interactions with Compartmentalized Cellular Phosphates Explain Rare Earth Oxide Nanoparticle Hazard and Provide Opportunities for Safer Design. ACS Nano. 2014; 8:1771–1783. [PubMed: 24417322]
28. Zhang H, Dunphy DR, Jiang X, Meng H, Sun B, Tarn D, Xue M, Wang X, Lin S, Ji Z, Li R, Garcia FL, Yang J, Kirk ML, Xia T, Zink JI, Nel A, Brinker CJ. Processing Pathway Dependence of Amorphous Silica Nanoparticle Toxicity: Colloidal Vs Pyrolytic. J Am Chem Soc. 2012; 134:15790–15804. [PubMed: 22924492]
29. Cevik IU, Dalkara T. Intravenously Administered Propidium Iodide Labels Necrotic Cells in the Intact Mouse Brain after Injury. Cell Death Differ. 2003; 10:928–929. [PubMed: 12868000]
30. Sydlik SA, Jhunjhunwala S, Webber MJ, Anderson DG, Langer R. *In Vivo* Compatibility of Graphene Oxide with Differing Oxidation States. ACS Nano. 2015; 9:3866–3874. [PubMed: 25849074]
31. Nishida E, Miyaji H, Kato A, Takita H, Iwanaga T, Momose T, Ogawa K, Murakami S, Sugaya T, Kawanami M. Graphene Oxide Scaffold Accelerates Cellular Proliferative Response and Alveolar Bone Healing of Tooth Extraction Socket. Int J Nanomed. 2016; 11:2265–2277.
32. Vera-Sanchez M, Aznar-Cervantes S, Jover E, Garcia-Bernal D, Onate-Sanchez RE, Hernandez-Romero D, Moraleda JM, Collado-Gonzalez M, Javier Rodriguez-Lozano F, Luis Cenis J. Silk-Fibroin and Graphene Oxide Composites Promote Human Periodontal Ligament Stem Cell

Spontaneous Differentiation into Osteo/ Cementoblast-Like Cells. Stem Cells Dev. 2016; 25:1742–1754. [PubMed: 27503546]

33. Garcia-Alegria E, Iluit M, Stefanska M, Silva C, Heeg S, Kimber SJ, Kouskoff V, Lacaud G, Vijayaraghavan A, Batta K. Graphene Oxide Promotes Embryonic Stem Cell Differentiation to Haematopoietic Lineage. Sci Rep. 2016; 6:25917. [PubMed: 27197878]
34. Jasim DA, Murphy S, Newman L, Mironov A, Prestat E, McCaffrey J, Menard-Moyon C, Rodrigues AF, Bianco A, Haigh S, Lennon R, Kostarelos K. The Effects of Extensive Glomerular Filtration of Thin Graphene Oxide Sheets on Kidney Physiology. ACS Nano. 2016; 10:10753–10767. [PubMed: 27936585]
35. Sasidharan A, Swaroop S, Koduri CK, Girish CM, Chandran P, Panchakarla LS, Somasundaram VH, Gowd GS, Nair S, Koyakutty M. Comparative *in Vivo* Toxicity, Organ Biodistribution and Immune Response of Pristine, Carboxylated and Pegylated Few-Layer Graphene Sheets in Swiss Albino Mice: A Three Month Study. Carbon. 2015; 95:511–524.
36. Roberts JR, Mercer RR, Stefaniak AB, Seehra MS, Geddam UK, Chaudhuri IS, Kyrlidis A, Kodali VK, Sager T, Kenyon A, Bilgesu SA, Eye T, Scabilloni JF, Leonard SS, Fix NR, Schwegler-Berry D, Farris BY, Wolfarth MG, Porter DW, Castranova V, Erdely A. Evaluation of Pulmonary and Systemic Toxicity Following Lung Exposure to Graphite Nanoplates: A Member of the Graphene-Based Nanomaterial Family. Part Fibre Toxic. 2016; 13:22.
37. Wen KP, Chen YC, Chuang CH, Chang HY, Lee CY, Tai NH. Accumulation and Toxicity of Intravenously-Injected Functionalized Graphene Oxide in Mice. J Appl Toxicol. 2015; 35:1211–1218. [PubMed: 26099253]
38. Duch MC, Budinger GRS, Liang YT, Soberanes S, Urich D, Chiarella SE, Campochiaro LA, Gonzalez A, Chandel NS, Hersam MC, Mutlu GM. Minimizing Oxidation and Stable Nanoscale Dispersion Improves the Biocompatibility of Graphene in the Lung. Nano Lett. 2011; 11:5201–5207. [PubMed: 22023654]
39. Samuel ELG, Marcano DC, Berka V, Bitner BR, Wu G, Potter A, Fabian RH, Pautler RG, Kent TA, Tsai AL, Tour JM. Highly Efficient Conversion of Superoxide to Oxygen Using Hydrophilic Carbon Clusters. Proc Natl Acad Sci U S A. 2015; 112:2343–2348. [PubMed: 25675492]
40. Mari E, Mardente S, Morgante E, Tafani M, Lococo E, Fico F, Valentini F, Zicari A. Graphene Oxide Nanoribbons Induce Autophagic Vacuoles in Neuroblastoma Cell Lines. Int J Mol Sci. 2016; 17:E1995. [PubMed: 27916824]
41. Mu QX, Su GX, Li LW, Gilbertson BO, Yu LH, Zhang Q, Sun YP, Yan B. Size-Dependent Cell Uptake of Protein-Coated Graphene Oxide Nanosheets. ACS Appl Mater Interfaces. 2012; 4:2259–2266. [PubMed: 22409495]
42. Huang J, Zong C, Shen H, Liu M, Chen B, Ren B, Zhang Z. Mechanism of Cellular Uptake of Graphene Oxide Studied by Surface-Enhanced Raman Spectroscopy. Small. 2012; 8:2577–2584. [PubMed: 22641430]
43. Zhang H, Peng C, Yang JZ, Lv M, Liu R, He DN, Fan CH, Huang Q. Uniform Ultrasmall Graphene Oxide Nanosheets with Low Cytotoxicity and High Cellular Uptake. ACS Appl Mater Interfaces. 2013; 5:1761–1767. [PubMed: 23402618]
44. Lammel T, Boisseaux P, Fernandez-Cruz ML, Navas JM. Internalization and Cytotoxicity of Graphene Oxide and Carboxyl Graphene Nanoplatelets in the Human Hepatocellular Carcinoma Cell Line Hep G2. Part Fibre Toxicol. 2013; 10:21. [PubMed: 23742083]
45. Zhu Y, Murali S, Cai W, Li X, Suk JW, Potts JR, Ruoff RS. Graphene and Graphene Oxide: Synthesis, Properties, and Applications. Adv Mater. 2010; 22:3906–3924. [PubMed: 20706983]
46. Georgakilas V, Otyepka M, Bourlinos AB, Chandra V, Kim N, Kemp KC, Hobza P, Zboril R, Kim KS. Functionalization of Graphene: Covalent and Non-Covalent Approaches, Derivatives and Applications. Chem Rev. 2012; 112:6156–6214. [PubMed: 23009634]
47. Garcia-Alegria E, Iluit M, Stefanska M, Silva C, Heeg S, Kimber SJ, Kouskoff V, Lacaud G, Vijayaraghavan A, Batta K. Graphene Oxide Promotes Embryonic Stem Cell Differentiation to Haematopoietic Lineage. Sci Rep. 2016; 6:25917. [PubMed: 27197878]
48. Tang Y, Scheef EA, Wang S, Sorenson CM, Marcus CB, Jefcoate CR, Sheibani N. Cyp1b1 Expression Promotes the Proangiogenic Phenotype of Endothelium through Decreased

Intracellular Oxidative Stress and Thrombospondin-2 Expression. Blood. 2009; 113:744–754. [PubMed: 19005183]

49. Li R, Wu Ra, Zhao L, Wu M, Yang L, Zou H. P-Glycoprotein Antibody Functionalized Carbon Nanotube Overcomes the Multidrug Resistance of Human Leukemia Cells. ACS Nano. 2010; 4:1399–1408. [PubMed: 20148593]
50. Li RB, Wang X, Ji ZX, Sun BB, Zhang HY, Chang CH, Lin SJ, Meng H, Liao YP, Wang MY, Li ZX, Hwang AA, Song TB, Xu R, Yang Y, Zink JI, Nel AE, Xia T. Surface Charge and Cellular Processing of Covalently Functionalized Multiwall Carbon Nanotubes Determine Pulmonary Toxicity. ACS Nano. 2013; 7:2352–2368. [PubMed: 23414138]

A

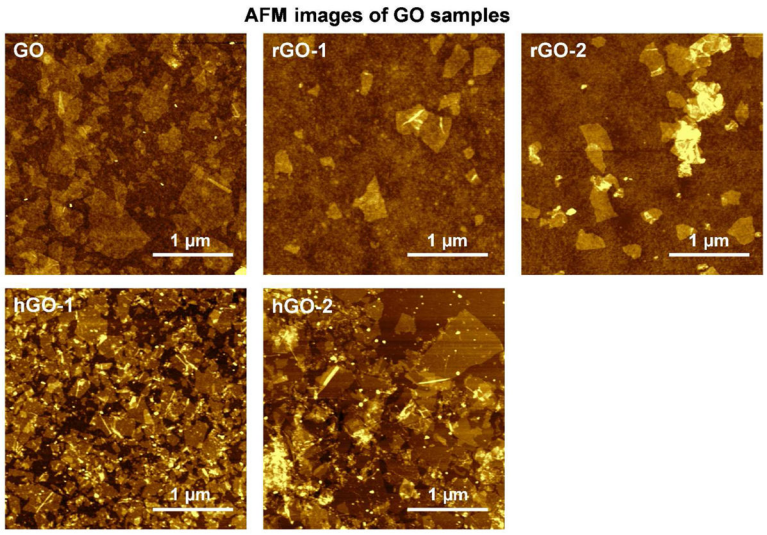

B

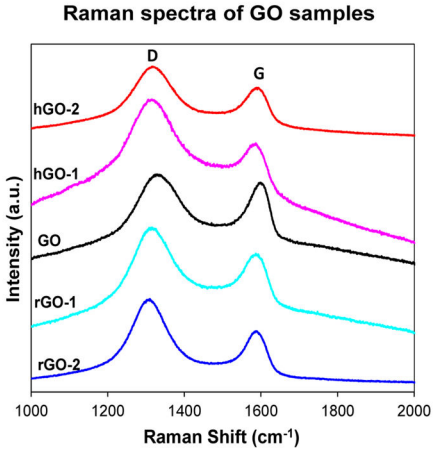

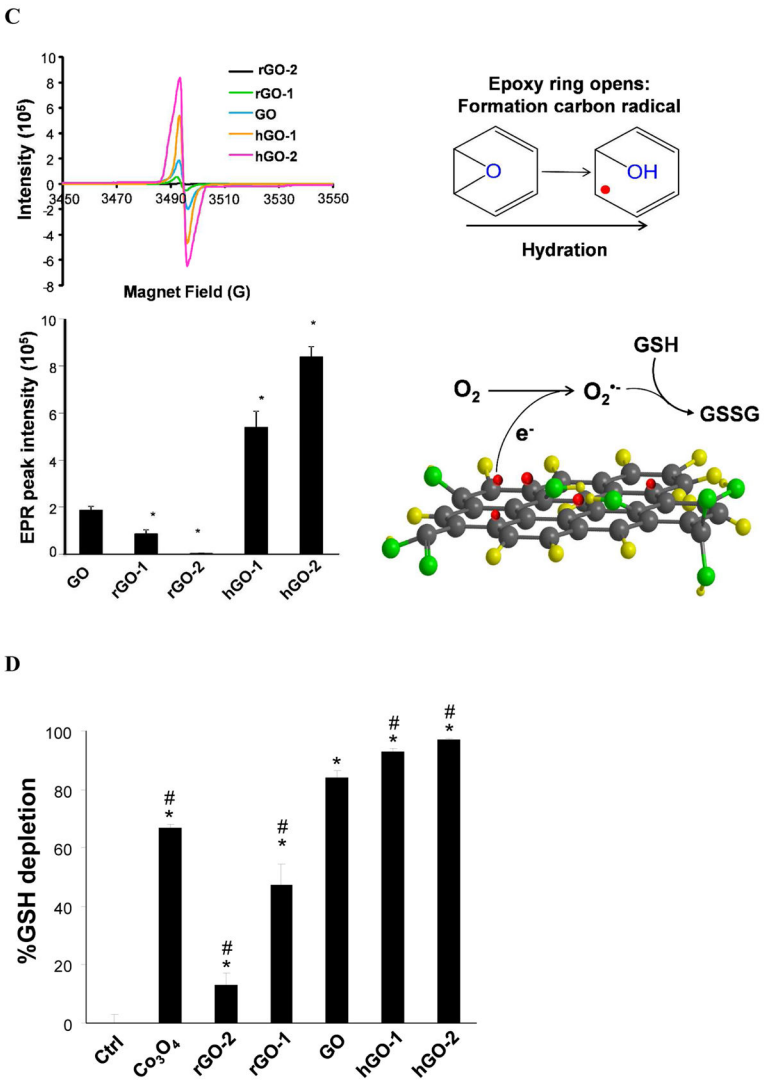

Figure 1. Characterization of the physicochemical properties of GO samples

(A) AFM images; (B) Confocal Raman spectra; (C) Assessment of carbon radical formation, quantification by EPR, and schematic describing the link to ROS generation; (D) Abiotic glutathione (GSH) assay. AFM samples were prepared by placing a drop of the GO solution on Si wafers that were pretreated with an APTES aqueous solution. After washing with water and drying under N_2, AFM images were obtained in an Asylum Cypher ES AFM, used in tapping mode with conical probes. Confocal Raman analysis was performed in a Renishaw in *Via* Raman microscope system equipped with a 514.5 nm Ar laser. Carbon radicals form during the hydration process, which leads to opening of epoxy rings by nucleophiles in the aqueous solution. The presence of carbon radicals was assessed by an X-band Bruker ELEXYS 580 electron paramagnetic resonance (EPR) spectrometer. The schematic shows how the reactive carbon radicals could generate superoxide in the presence of molecular dioxygen, with subsequent ability to oxidize the GSH thiol groups. An abiotic GSH-Glo™ glutathione assay was used to assess the pro-oxidative potential of GO samples by luminescence measurement in a SpectraMax M5 microplate spectrophotometer.

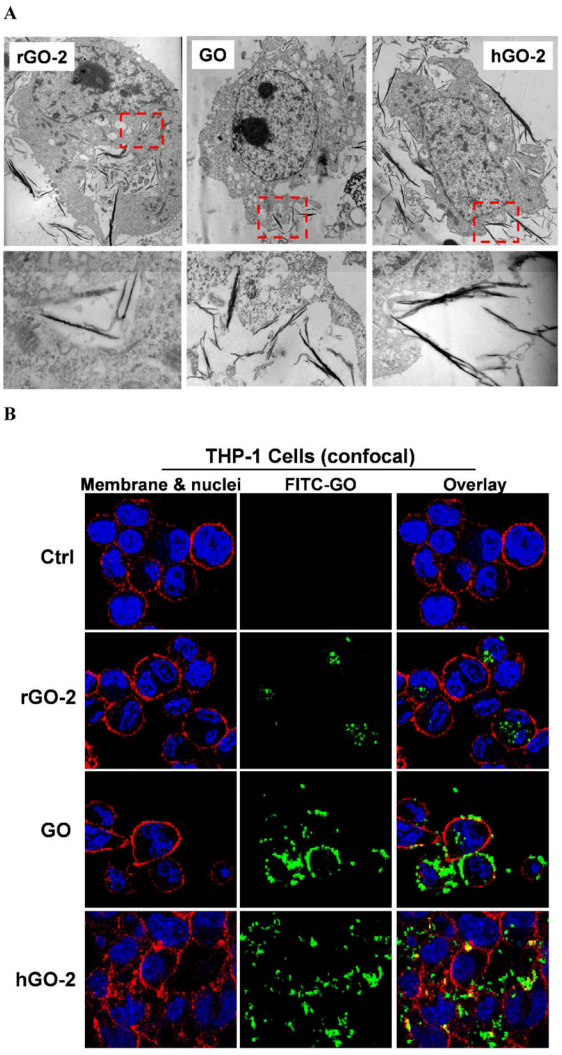

Figure 2. Determination of the cellular interactions with the functionalized GO nanosheets

(A) Visualizing the interactions of GO with THP-1 cells by TEM; (B) confocal imaging of FITC-BSA labeled GO samples in BEAS-2B cells. After exposure to rGO-2, GO or hGO-2 for 16 h, the cells were washed, fixed and stained for TEM viewing, as described in the Method section. For confocal viewing of the interactions of the labeled nanosheets with the cells, the various GO samples were incubated with the cells at 25 μg/mL for 16 h before washing and staining with Hoechst 33342 dye (blue) and Alexa fluor 594-labeled WGA antibody. Samples were viewed under a confocal microscope (Leica Confocal SP2 1P/FCS).

A

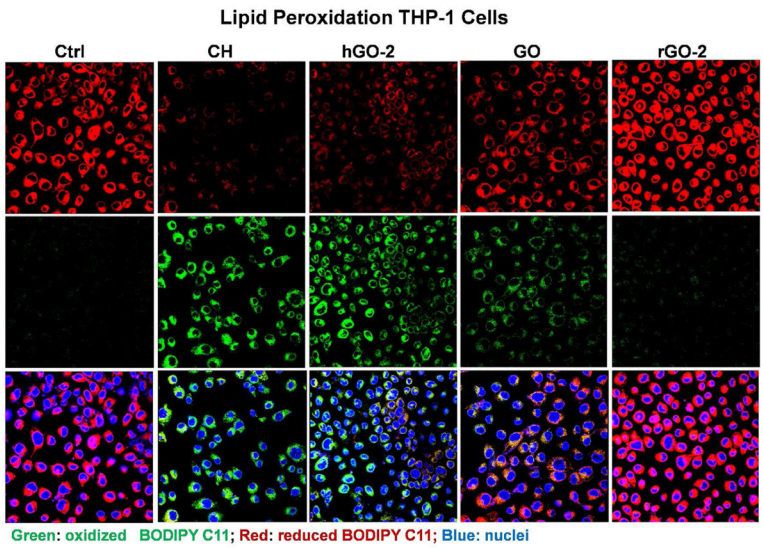

B

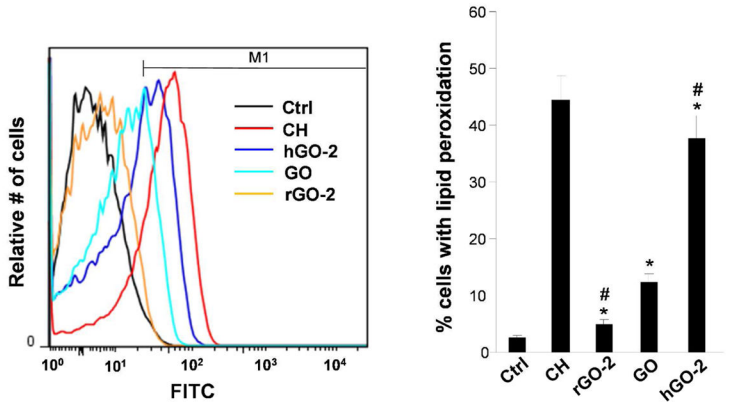

C

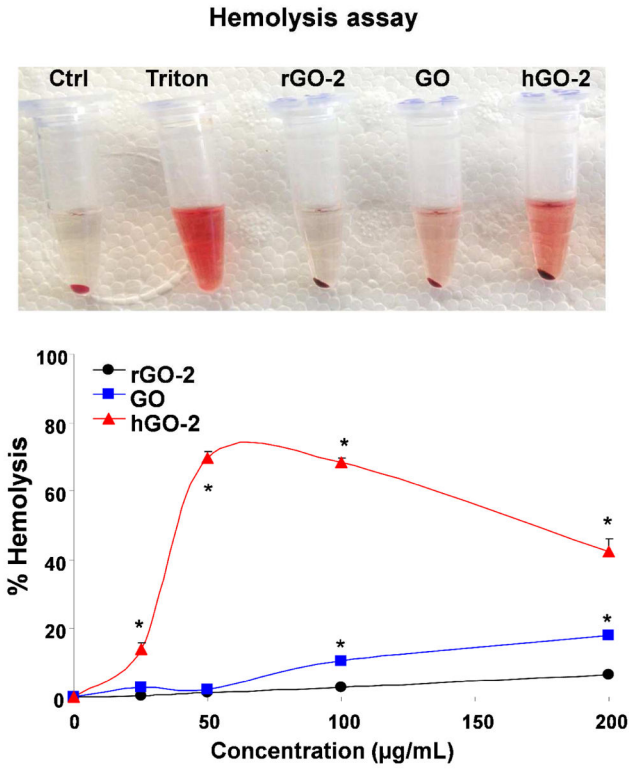

Figure 3. Assessment of the lipid peroxidation and hemolygis by GO nanosheets

(A) Confocal images to demonstrate the generation of lipid peroxidation by the various GO samples; (B) flow cytometry assessment to quantify the percentage of cells undergoing lipid peroxidation; (C) Red blood cell hemolysis by GO samples. To assess lipid peroxidation, THP-1 cells were treated with 100 μg/mL GO for 16 h or 10 μM cumene hydroperoxide (positive control) for 1 h. Cells were stained with 10 SM Image-iT® Lipid Peroxidation Sensor Lipid Peroxidation Sensor according to the manufacturer's instructions, as well as co-stained with Hoechst 33342 for 30 min. After staining and washing, fluorescence readings were recorded to assess the reduction or oxidation status of the dye at excitation/emission wavelengths of 581/591 nm (Texas Red® filter set) and 488/510 nm (traditional FITC filter), respectively. Flow cytometry analysis was carried out in a FACS Vantage SE flow cytometer. The hemolysis assay was performed by incubation of freshly prepared mouse red blood cells with GO nanosheets. Following RBC centrifugation, the supernatants were collected and hemoglobin content was determined by measuring absorbance at 540 nm using a UV-VIS spectrometer. *$p < 0.05$ compared to Ctrl, #$p < 0.05$ compared to pristine GO.

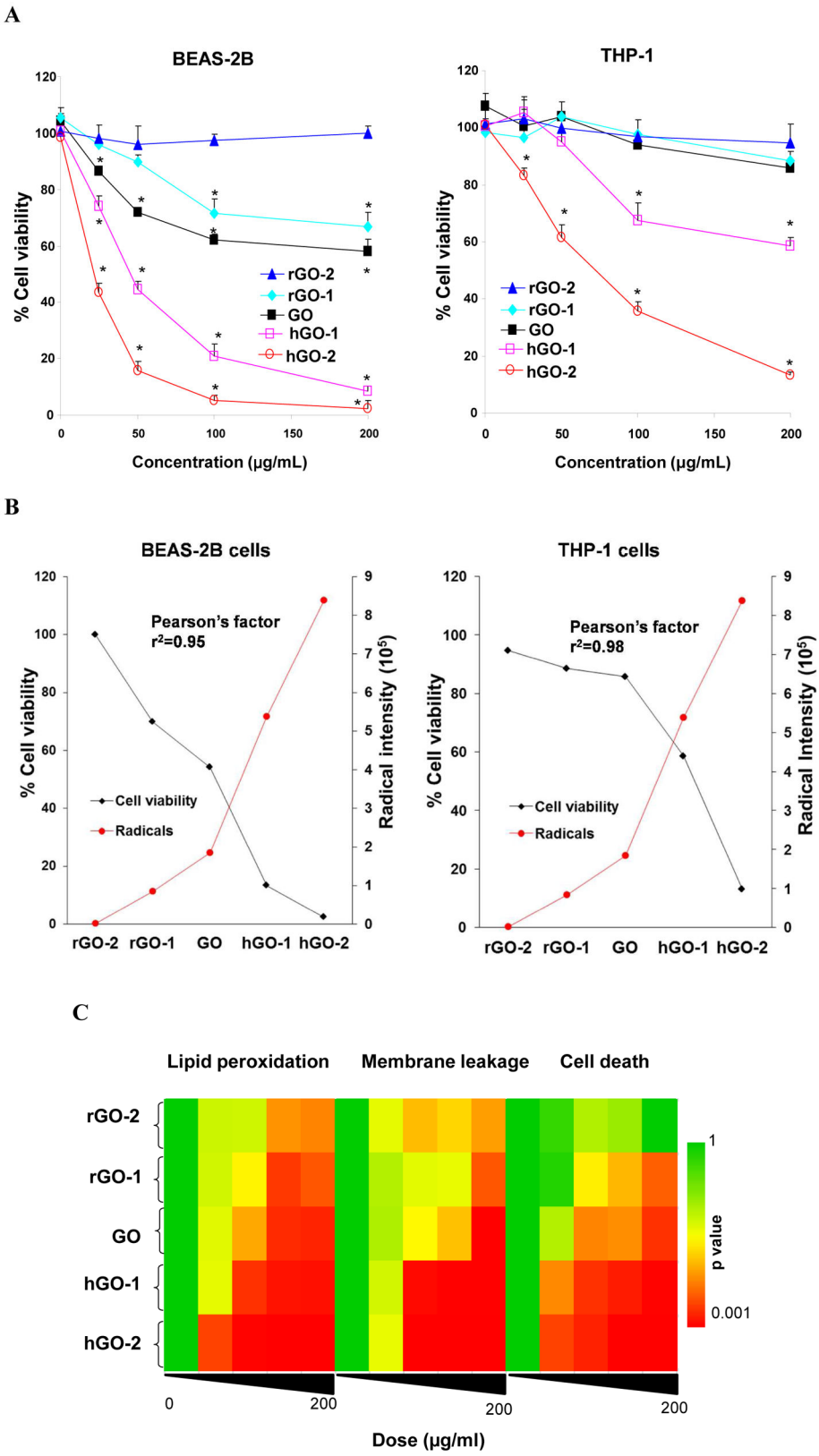

Figure 4. Assessment of the cytotoxicity of the library of GO materials

(A) Cell viability assessment in in THP-1 and BEAS-2B cells by the MTS assay; (B) Calculation of the correlation coefficient of the cytotoxicity results *versus* carbon radical measurement; (C) heat map display to show the hierarchical ranking of the effects of the various library materials on cellular toxicity, membrane peroxidation and RBC leakage. For cellular viability assessment, a MTS assay was used to assess the impact of 0–200 μg/mL of each GO suspension in THP-1 or BEAS-2B cells over 48h. *$p < 0.05$ compared to Ctrl, #$p < 0.05$ compared to pristine GO. The heat maps were established using one-way ANOVA analysis to evaluate the different cellular response parameters at 0–200 μg/mL, as described in the Methods section. *$p < 0.05$ compared to Ctrl, #$p < 0.05$ compared to pristine GO.

A

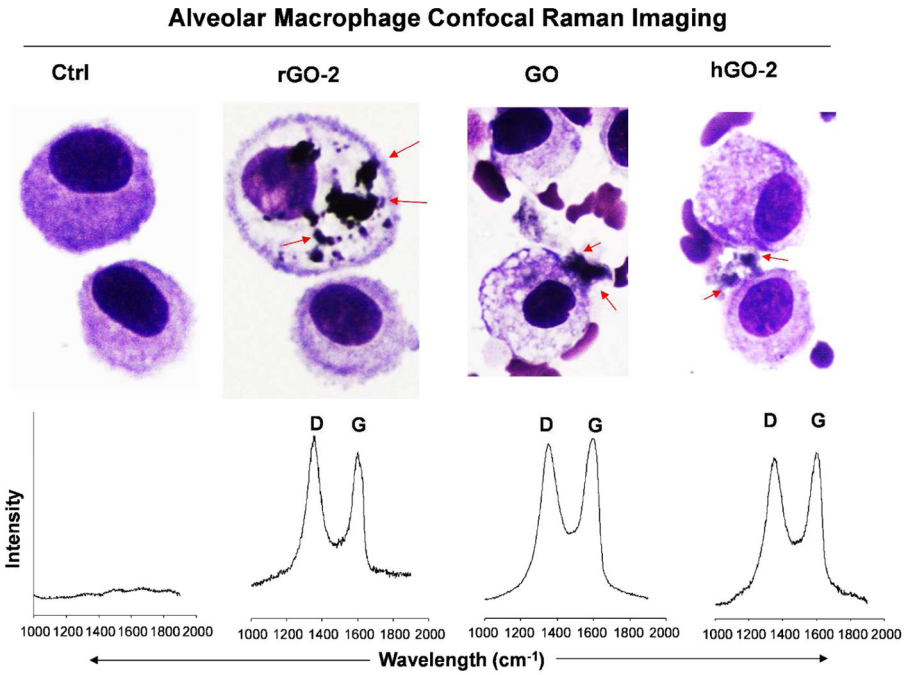

B

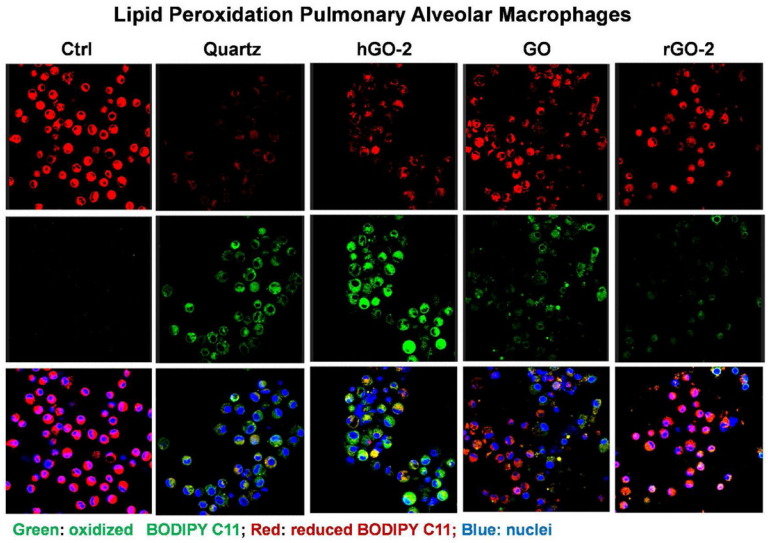

C

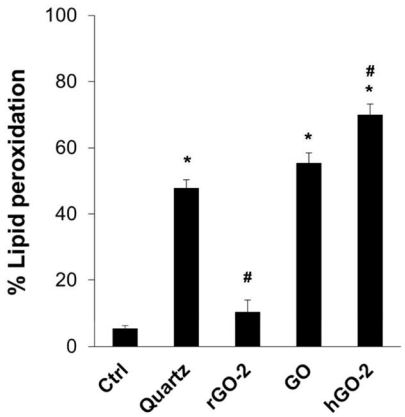

D

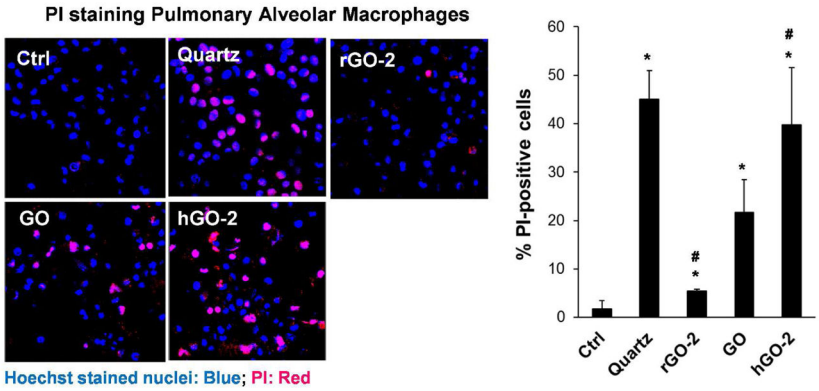

Figure 5. Lipid peroxidation and cell death of primary macrophages in the BALF after GO exposure by oropharyngeal aspiration

(A) Raman microscopy to assess the uptake of GO by BALF macrophages; (B) Confocal imaging to assess lipid peroxidation in BALF macrophages; (C) Flow cytometry analysis to quantify the percentage of cells undergoing lipid peroxidation; (D) PI staining to assess membrane permeability in primary alveolar macrophages. Animal exposure to rGO-2, GO and hGO-2 nanosheets was performed by using oropharyngeal aspiration of 2 mg/kg of each of the samples. Animals were sacrificed after 40 h to collect primary alveolar macrophages. Typical G and D bands of GO nanosheets were obtained by conducting confocal Raman microscopy. To determine the percentage of PI-positive cells, the recovered BALF macrophages were seeded in 8-well chamber or 6-well plate for 2 h, stained with 1 μg/mL PI and fixed for confocal imaging. *$p < 0.05$ compared to Ctrl, #$p < 0.05$ compared to pristine GO.

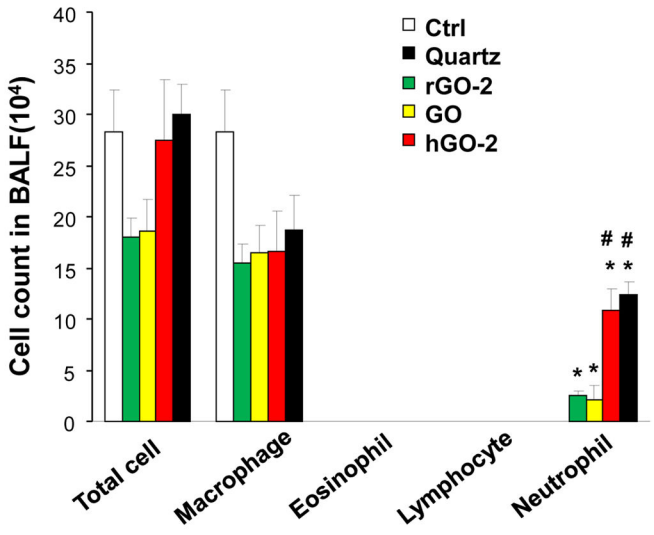

B

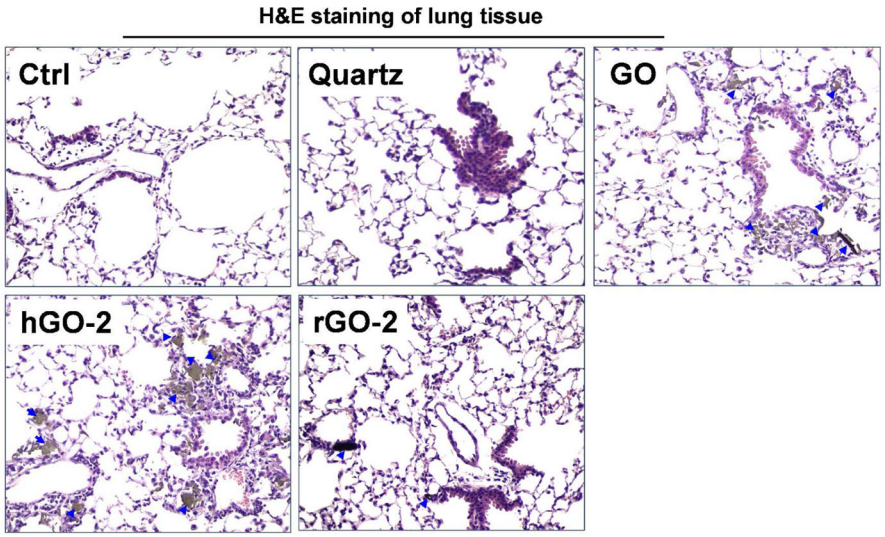

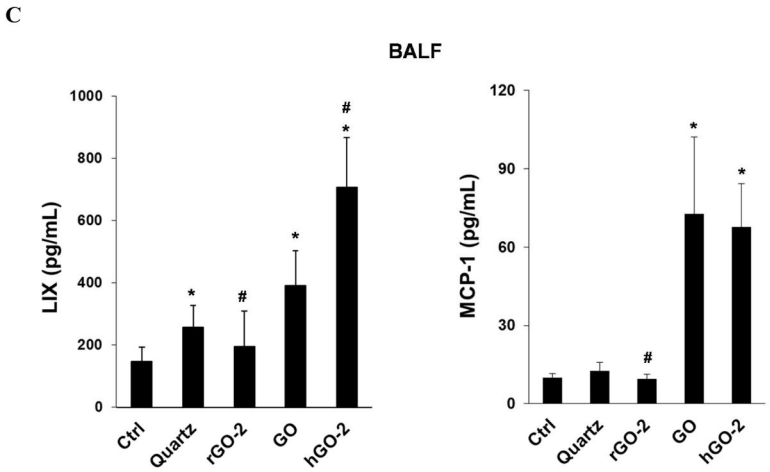

Figure 6. Induction of acute lung inflammation induced by the various GO materials

(A) Differential cell counts in the BALF of exposed animals; (B) H&E staining to visualize pulmonary inflammation (arrows represent GO flakes); (C) Cytokine release in the BALF. BALF was collected from animals exposed to 2 mg/kg of the various GO sheets for 40 h, as described in Figure 5. MCP-1 and LIX levels in the BALF were analyzed by ELISA. *$p < 0.05$ compared to Ctrl, #$p < 0.05$ compared to pristine GO.

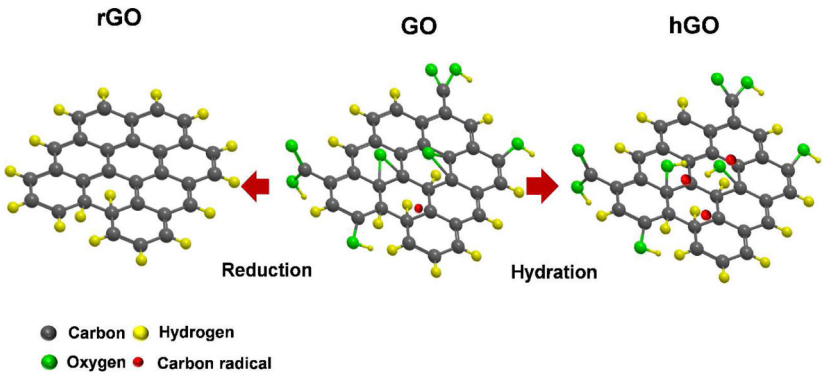

Scheme 1. Scheme illustrating the synthesis of reduced and hydrated GO samples

Pristine GO was prepared by a modified Hummers' method. Reduced GO materials were synthesized by solvothermal reduction of GO in NMP at 150 °C for 1 or 5 h. Hydrated GO nanosheets were prepared by hydrolysis in an aqueous alkalized solution at 50 °C or 100 °C for 24 h. Surface reduction decreases surface oxidation levels, while hydration has the opposite effect.

Table 1

Zeta potential and Hydrodynamic size of *f*-GO in different media

Nanoparticles		GO	rGO-1	rGO-2	hGO-1	hGO-2
Hydrodynamic Size (nm)	Water	334.1 ± 3.1	378.1 ± 3.9	549.2 ± 1.5	307.5 ± 6.7	329.8 ± 7.0
	BEGM	589.4 ± 23.2	596.5 ± 14.3	596.4 ± 2.4	546.7 ± 10.2	555.1 ± 38.4
	RPMI	321.5 ± 6.5	432.1 ± 27.4	456.5 ± 5.1	337.8 ± 9.8	340.8 ± 25.0
Zeta Potential (mV)	Water	−51.7 ± 0.9	−36.3 ± 1.4	−24.4 ± 0.7	−50.6 ± 0.8	−49.4 ± 0.9
	BEGM	−18.5 ± 0.6	−8.7 ± 2.7	−8.2 ± 2.2	−16.7 ± 0.8	−14.7 ± 2.5
	RPMI	−7.5 ± 0.5	−5.5 ± 1.2	−6.5 ± 3.6	−7.9 ± 3.9	−6.4 ± 2.2

Table 2

GO surface functional groups, carbon radical density and defect levels

		rGO-2	rGO-1	GO	hGO-1	hGO-2
XPS (atomic %)	Total oxygen	16.5	21.2	36.7	30.2	27.8
	C-OH	4.1	5.3	6.8	11.3	14.5
	C=O	8.3	8.8	9.4	10.7	12.2
	C-O-C	4.1	7.4	20.5	9.2	1.1
EPR (10^5)	•C	0.01	0.84	1.85	5.38	8.38
Raman (I_D/I_G)	Defects	1.07	1.13	1.17	1.05	0.95